Available online at www.sciencedirect.com
ScienceDirect
Geochimica et Cosmochimica Acta 70 (2006) 5253–5269
Geochimica
www.elsevier.com/locate/gca

Cd adsorption onto *Anoxybacillus flavithermus*: Surface complexation modeling and spectroscopic investigations

Peta-Gaye G. Burnett [a,*], Christopher J. Daughney [b], Derek Peak [a]

[a] *Department of Soil Science, University of Saskatchewan, 51 Campus Drive, Saskatoon, Sask., Canada S7N 5A8*
[b] *Institute of Geological and Nuclear Sciences, P.O. Box 30368, Lower Hutt, New Zealand*

Received 1 February 2006; accepted in revised form 3 August 2006

Abstract

Several recent studies have applied surface complexation theory to model metal adsorption behaviour onto mesophilic bacteria. However, no investigations have used this approach to characterise metal adsorption by thermophilic bacteria. In this study, we perform batch adsorption experiments to quantify cadmium adsorption onto the thermophile *Anoxybacillus flavithermus*. Surface complexation models (incorporating the Donnan electrostatic model) are developed to determine stability constants corresponding to specific adsorption reactions. Adsorption reactions and stoichiometries are constrained using spectroscopic techniques (XANES, EXAFS, and ATR–FTIR). The results indicate that the Cd adsorption behaviour of *A. flavithermus* is similar to that of other mesophilic bacteria. At high bacteria-to-Cd ratios, Cd adsorption occurs by formation of a 1:1 complex with deprotonated cell wall carboxyl functional groups. At lower bacteria-to-Cd ratios, a second adsorption mechanism occurs at pH > 7, which may correspond to the formation of a Cd–phosphoryl, CdOH–carboxyl, or CdOH–phosphoryl surface complex. X-ray absorption spectroscopic investigations confirm the formation of the 1:1 Cd–carboxyl surface complex, but due to the bacteria-to-Cd ratio used in these experiments, other complexation mechanism(s) could not be unequivocally resolved by the spectroscopic data.

1. Introduction

The adsorption of metals by bacteria can influence the speciation and mobility of metals in geologic and aquatic environments. Previous studies of metal–bacteria adsorption have utilised surface complexation theory to quantify the amount of metal adsorbed (e.g., Fein et al., 1997; Daughney and Fein, 1998; Daughney et al., 1998; Fowle and Fein, 1999, 2000; Fein et al., 2001; Daughney et al., 2001; Yee and Fein, 2001; Yee et al., 2004a,b). Surface complexation theory is a specific type of chemical equilibrium approach that correlates experimental adsorption data with electrical double layer (EDL) theory and bonding mechanisms to describe adsorption. Surface complexation models (SCMs) explicitly describe the chemical reactions that occur between the solute and specific sites on the surface of interest (e.g., carboxylic, phosphoryl, hydroxyl, amino, etc.) (Beveridge et al., 1982; Fein et al., 1997; Daughney et al., 1998; Fowle et al., 2000; Fein et al., 2001; Yee and Fein, 2001). Most SCMs constructed for metal biosorption are primarily based on macroscopic data, and only a limited number of investigations have used spectroscopic techniques to identify the functional groups on microbial surfaces (Sarret et al., 1998; Kelly et al., 2001, 2002; Boyanov et al., 2003; Benning et al., 2004; Sheng et al., 2004; Wei et al., 2004; Yee et al., 2004a,b). Obtaining direct evidence of the reaction mechanisms involved in metal biosorption and the chemical composition of the metal–bacterial complexes formed is vital for validation of SCMs.

Despite the importance of metal–microbe interactions, no extensive metal adsorption investigations have been conducted on thermophilic bacteria. Thermophiles are extremophilic microorganisms that have adapted to grow at elevated temperatures ranging from approximately 45

* Corresponding author. Fax: +1 30 69 666 881.
E-mail address: pete.burnett@usask.ca (P.-G. G. Burnett).

0016-7037/$ - see front matter © 2006 Elsevier Inc. All rights reserved.
doi:10.1016/j.gca.2006.08.002

to 80 °C (Brock, 1986; Madigan, 2000; Chapelle, 2001; Sampson and Phillips, 2001). It is unknown whether the metal adsorption behaviour of thermophiles parallels the adsorption behaviour of bacteria grown at lower temperatures and/or if the binding capacity of thermophiles is greater or lesser than that of mesophiles.

In this investigation, we conduct Cd adsorption experiments using the model thermophile *Anoxybacillus flavithermus* cultured to late stationary phase. We describe the experimental data by using SCMs that incorporate the Donnan shell electrostatic model, with the aim of quantifying Cd-binding constants. These SCMs include reactions for proton adsorption as described in Burnett et al. (2006). X-ray absorption (XAS) and Fourier Transform infrared (FTIR) spectroscopy are used to constrain SCM reactions and stoichiometries. Our objectives are (1) to provide a set of SCM parameters that describe Cd interactions with the selected thermophile, (2) to identify the reaction mechanisms occurring between Cd and the thermophile, and (3) to compare the Cd binding characteristics to those observed for mesophilic Gram-positive and Gram-negative bacteria previously described in the literature.

Cadmium was selected as the model metal because it is among the most common heavy metal pollutants and is a potential toxicant found in effluent from manufacturing, construction, chemical, and agricultural industries (Sheng et al., 2004). Additionally, Cd adsorption by various mesophilic bacteria has been previously described (e.g., Fein et al., 1997; Daughney and Fein, 1998; Daughney et al., 1998; Fowle and Fein, 1999, 2000; Daughney et al., 2001; Yee and Fein, 2001; Boyanov et al., 2003; Borrok et al., 2004a,b; Borrok and Fein, 2005), and as such, comparisons to *A. flavithermus* can be made. Furthermore, Cd is an experimentally simple metal to work with because precipitates are not expected to form under the conditions of the experiments performed in this investigation.

2. Methods

2.1. Growth procedures

Anoxybacillus flavithermus was isolated from the main wastewater drain at the Wairakei Geothermal Power Station (New Zealand). The bacterial species was prepared and cultured following the procedure outlined in Burnett et al. (2006). *A. flavithermus* grown by this protocol has a surface area of $7.92\ m^2\ g^{-1}$ and a cell wall thickness of 28.1 ± 7.4 nm, respectively. The cell wet to dry weight ratio is 6.7 ± 0.1 to 1 and the dry biomass present in a suspension is 0.5359 times its corresponding optical density at 600 nm (OD_{600}).

Bacterial cells were examined before and after Cd adsorption experiments using a Bio-Rad MRC-1000 confocal scanning system (Hemel Hempstead, UK) equipped with a krypton–argon laser and mounted on a Nikon Mircophot-SA microscope (Tokyo, Japan). Cells were fixed by flaming, stained with syto-9 and propydium iodide, and then viewed through a 60× oil immersion lens. To investigate the possible release of exudates and metabolites from cells during Cd adsorption, dissolved organic carbon (DOC) concentrations were measured in filtrates (0.45 μm) of bacterial suspensions collected after 2 h equilibration with Cd ($5\ mg\ L^{-1}$) at various pHs and ionic strengths. These results were compared to control experiments performed by Burnett et al. (2006). All DOC analyses were performed using a Shimadzu TOC 5050A total organic carbon analyser (Kyoto, Japan) employing a non-purgeable organic carbon method.

2.2. Cadmium kinetics and reversibility

Adsorption kinetics experiments were conducted over the pH range 5–7. Within 15 min of the final rinse, the bacterial pellet was resuspended in a known weight of 0.01 M $NaNO_3$. The suspension was then homogenised by vigorous shaking (15 min) and the OD_{600} recorded for calculation of the bacterial concentration. A known mass of $1000\ mg\ L^{-1}$ Cd (Merck, $Cd(NO_3)_2$ in 0.5% HNO_3) standard solution was added to yield an initial Cd concentration of $5\ mg\ L^{-1}$. The pH of the suspension was adjusted to the desired value using 0.1 M NaOH. Aliquots (5 mL) of the suspension were transferred to polypropylene reaction vessels, which were then placed in an orbital mixer incubator (100 rpm) to provide agitation. All adsorption experiments were performed at 25 °C to ensure that results would be comparable to previous experiments conducted with mesophilic bacteria. Samples were removed from the incubator at various time intervals after agitation began and immediately centrifuged at 6870*g* for 15 min. The supernatant was acidified with two drops of concentrated HNO_3 solution (ARISTAR grade) to prevent Cd precipitation before or during the analysis for dissolved Cd by flame atomic absorption spectrophotometry (FAAS) (Perkin-Elmer *AAnalyst 800*, Rodgau-Jügesheim, Germany). The reversibility of adsorption was assessed using samples that had undergone prior equilibration at pH ~7 with $5\ mg\ L^{-1}$ Cd for 2 h, based on a well-established experimental protocol (Fein et al., 1997; Fowle and Fein, 2000; Yee and Fein, 2001; Châtellier and Fortin, 2004; Borrok and Fein, 2005).

2.3. Cadmium adsorption

Washed bacteria were resuspended in electrolyte to form a parent suspension which was used to prepare two additional suspensions with approximately 0.5 and 0.25 times the original biomass concentration (the electrolyte was used as the diluent). Experiments were conducted at fixed initial Cd concentrations ($5\ mg\ L^{-1}$) and as a function of pH (3.6–9.7) and solid-to-solution ratio (0.07–1.09 dry $g\ L^{-1}$). Samples were allowed to equilibrate while shaking for 2 h (based on the results of the kinetics experiments), followed by centrifugation (6870*g*, 15 min or 3522*g*, 30 min). Sampling techniques were identical to those previously described and the final concentration of

dissolved Cd was determined by FAAS (Perkin-Elmer *AAnalyst 800*, Rodgau-Jügesheim, Germany or Varian Spectr*AA* 220, Victoria, Australia) or Inductively Coupled Plasma Optical Emission Spectroscopy (ICP-OES) (Thermo Jarrell Ash IRIS spectrophotometer, USA). A similar protocol has been employed by other researchers (Fein et al., 1997; Daughney and Fein, 1998; Daughney et al., 1998; Fowle and Fein, 1999; Daughney et al., 2001; Yee and Fein, 2003; Borrok et al., 2004a,b; Yee et al., 2004a,b; Borrok and Fein, 2005).

2.4. Modeling

A modified version (FITMOD) of the computer program FITEQL 2.0 (Westall, 1982) was used to construct SCMs describing Cd interactions with *A. flavithermus*. SCMs developed in this investigation incorporated the Donnan electrostatic model, in which the ionisable functional groups are assumed to be distributed uniformly throughout a volume (Martinez et al., 2002). The Donnan model has been successfully employed to quantify the extent of ion–bacteria adsorption over a wide range of pH, ionic strength conditions, and solute-to-sorbent ratios (Ohshima and Kondo, 1991; Ohshima, 1995; Plette et al., 1995; van der Wal et al., 1997; Wonders et al., 1997; Wasserman and Felmy, 1998; Martinez et al., 2002; Ohshima, 2002; Daughney et al., 2004; Yee et al., 2004a,b). FITMOD calculates the overall variance $V(Y)$ of the error (Y) in the chemical mass balance equations and therefore provides a quantitative estimate of the accuracy of the fit. For SCMs involving mineral surfaces, values of $V(Y)$ between 1 and 20 indicate reasonable fits to the data (Westall, 1982).

Deprotonation reactions for surface functional groups and interactions of metal cations (M^m) with deprotonated surface functional groups were modeled by the following general chemical reaction and mass action law:

$$R - L_nH^x \Longleftrightarrow R - L_n^{x-1} + H^+ \quad (1)$$

$$K_n = \frac{\left[R - L_n^{x-1}\right] a_{H^+}}{\left[R - L_nH^x\right]} \quad (2)$$

$$R - L_n^{x-1} + M^m \Longleftrightarrow R - L_nM^{(m+x-1)} \quad (3)$$

$$K_{M-n} = \frac{\left[R - L_nM^{(m+x-1)}\right] a_{H^+}}{\left[R - L_n^{x-1}\right] a_{M^m}} \quad (4)$$

where R represents the bacterial cell wall to which the functional group L_nH is attached, x represents the charge of the protonated functional group, K_n represents the deprotonation stability constant, brackets represent the concentration of the surface sites (mol L^{-1}), a_{H^+} represents the activity of protons, and K_{M-n} denotes the thermodynamic stability constant of the bacteria–metal complex. The effect of the bacterial surface electric field on protonation and metal adsorption reactions is accounted for using the following equation (Stumm and Morgan, 1996):

$$K_n^{int} = K_n \exp\left(\frac{-ZF\psi_D}{RT}\right) \quad (5)$$

Here, K_n^{int} is the intrinsic equilibrium constant referenced to zero for both surface charge and surface coverage. The variables Z, F, ψ_D, R, and T refer to the charge of the adsorbing ion, Faraday's constant, the electric potential at the location of adsorption (i.e., the Donnan potential), the gas constant, and the absolute temperature, respectively. These formulations have been successfully employed to describe proton and metal adsorption onto bacteria (Fein et al., 1997; Daughney and Fein, 1998; Daughney et al., 1998, 2001; Wightman et al., 2001; Yee and Fein, 2001; Borrok et al., 2004a,b; Borrok and Fein, 2005; Burnett et al., 2006).

In this study, all SCMs include proton adsorption reactions as described in Burnett et al. (2006). Specifically, proton adsorption involves a three pK_a SCM in which sites inferred to be carboxyl, phosphoryl, and amino sites become deprotonated (see Table 1). All SCMs include equilibria describing the dissociation of water, the acid, the base, and the electrolyte. SCMs also consider hydrolysis of Cd and Cd complexation by carbon dioxide, with stability constants taken from the Critical Stability Constants Database (Smith and Martell, 1976). All stability constants are adjusted for ionic strength using the Davies equation (Langmuir, 1997), and all values tabulated in this paper are referenced to zero ionic strength, zero surface charge, and 25 °C. SCM values for stability constants are determined for several independent batch adsorption sets, and the results are used to calculate uncertainties (weighted 2σ errors). Additionally, all SCMs are constructed using only Cd adsorption data corresponding to between 10% and 90% adsorption and pH $\leqslant$ 9. This modeling approach was followed to avoid biasing SCMs by consideration of data outside the 10–90% adsorption range and/or under pH conditions, where loss of Cd due to precipitation is predicted (Yee et al., 2004a,b).

2.5. X-ray absorption spectroscopy analyses

2.5.1. Standards and bacterial samples

Solution standards containing 50 mM Cd included samples of cadmium acetate and cadmium perchlorate of different compositions and concentrations. The ratio of Cd to anion was 1:2 in the cadmium perchlorate solution

Table 1
Average surface characteristics of *A. flavithermus* (Burnett et al., 2006)

Reaction	pK_a[a]	Site concentration[b]
$R–COOH \Longleftrightarrow R–COO^- + H^+$	4.94 ± 0.35	5.33 ± 0.87
$R–PO_4H \Longleftrightarrow R–PO_4^- + H^+$	6.85 ± 0.57	1.79 ± 0.84
$R–NH_3^+ \Longleftrightarrow R–NH_2 + H^+$	7.85 ± 0.27	1.42 ± 0.30

[a] Negative log$K$ values for the surface functional group, with 2σ errors, corresponding to zero ionic strength and zero surface coverage.
[b] Absolute concentrations of the surface functional group, with 2σ errors, in $\times 10^{-4}$ moles per gram dry bacteria.

(pH 5.2), and 1:2 and 1:50 in the cadmium acetate solutions (pH 7.3 and 5.7, respectively). All solution samples were transferred into liquid cells.

The bacterial pellets from a set of eighteen independently grown 400-mL cultures were combined to make three samples (pHs 3.9, 5.8, and 7.0), while a different set of eighteen cultures were combined to make three other samples (pHs 5.2, 7.6, and 8.5). Each sample (400 mL) was exposed to 5 mg L^{-1} Cd and the pH adjusted to the desired value using 1 M NaOH. After agitation for 2 h, samples were centrifuged (6079*g*, 15 min) and the supernatant decanted. The bacterial residues were filtered (0.45 μm) during centrifugation (3522*g*, 30 min) two more times to ensure maximum removal of entrained solution. The final concentration of dissolved Cd was determined by FAAS (Varian Spectr*AA* 220, Victoria, Australia) as described previously. Bacterial pellets were loaded directly into a slotted sample holder, sealed with kapton tape, and cooled to 77 K using liquid N_2. This experimental method is analogous to that employed by Kelly et al. (2001), Kelly et al. (2002), and Boyanov et al. (2003) for EXAFS on microbial systems. Note that the Cd loading was too low to obtain a reasonable signal from the pH 3.9 sample and so it will not be presented in this paper. Additionally, the pH 7.6 sample was excluded because of poor data quality (unknown cause). From this point forward, the pH 5.2 and 5.8 samples will be referred to as the pH 5 and 6 samples, respectively.

2.5.2. Data collection and analysis

XANES and EXAFS spectra were collected at the Advanced Photon Source at Argonne National Laboratory with the electron storage ring operating at 4.5 GeV and in top up mode (100 ± 0.5 mA) for all experiments. Measurements at the Cd K-edge (26.711 keV) were made on the PNC-CAT 20-BM beamline using a Si(111) reflection of the double crystal monochromator and with no focusing optics. Standards were analysed at room temperature in transmission mode. Energy calibration for solution standards was carried out by measuring the absorption of $Cd_3(PO_4)_2$ simultaneously with that of the sample. Biomass samples were placed in a cryostat and analysed at 77 K using a multi-element detector cooled with liquid N_2. Energy was calibrated using a reference Ag foil for solid standards and biomass samples. In all cases, multiple scans were collected to improve signal to noise ratio. Data analysis was carried out using WINXAS 3.1. Prior to processing the data, multiple scans were averaged. Calibration and background subtraction using standard procedures were always executed. Radial structure functions (RSFs) were generated by Fourier Transformation of the normalised, weighted $k^3\chi(k)$ data over an approximate k range of 2–9.5 $Å^{-1}$. The EXAFS oscillations were quantitatively analysed by curve fitting the data in *R*-space (out to 4.5 and 3.5 Å for standards and biomass samples, respectively) to theoretical scattering paths using FEFF 7.0. Uncertainties (2σ) in each parameter were estimated by taking the standard deviations of fits constructed for each scan (standards) and for the averages of fewer scans (biomass samples). These standard deviations provide a measure of precision not accuracy.

2.6. Fourier transform infrared spectroscopy analyses

2.6.1. Standards and bacterial samples

Solutions (50 mM) of $H_2PO_4^-$, HPO_4^{2-}, and PO_4^{3-} were prepared by dissolving the appropriate sodium phosphate salt in 18.2 MΩ deionized H_2O (Barnstead NanoPure, USA). Solutions of H_3PO_4 (50 mM) with and without 1 M $Cd(NO_3)_2$ were also prepared and both samples acidified with 0.75 mL concentrated HNO_3. Multiple 50 mM lecithin:Cd samples were prepared with molar ratios 1:0 and 1:2. A range of pH values (2.6–10.5) were obtained by addition of 1 M HNO_3 or 1 M NaOH. Note that lecithin ($R_1R_2HPO_4$) is a mixture of phospholipids and that R_1 and R_2 refer to $(CH_2)_2N(CH_3)_3$ and $CH_2CHR_3CH_2R_3$, respectively, where the latter bears hydrocarbon chains (R_3) of varying lengths. We estimated a molecular weight of 750 U assuming the main R_3-group is linoleic acid.

For bacterial sorption samples, the pellets from six independently grown 400-mL cultures were combined to provide sufficient biomass for the experiments and to eliminate interculture variability. After the final rinse step, washed bacteria were resuspended in a known volume of electrolyte and then divided among two reaction vessels of 400 mL each. One of the samples was exposed to 0.5 mM Cd and both samples adjusted to the desired pH. Samples were centrifuged (6079*g*, 15 min) after agitation for 2 h. The supernatant was decanted and analysed for dissolved Cd content via FAAS as described previously.

2.6.2. Data collection and analysis

FTIR experiments were performed on a Bruker Equinox 55 Infrared Spectrometer (Ettlingen, Germany) equipped with a purge gas generator and a mercury cadmium telluride (MCT) detector. Liquid samples (~1 mL) and wet bacterial pastes were loaded directly into a multiple bounce horizontal attenuated total reflectance (ATR) cell (Pike Technologies, USA) equipped with a 45 degree germanium (Ge) ATR crystal. Spectra were collected from 4000 to 700 cm^{-1} using 4 cm^{-1} resolution and 1024 co-added scans per sample. The ATR crystal was thoroughly cleaned with distilled H_2O and 95% ethanol between samples. The sample chamber was continuously purged using H_2O and CO_2-free air to improve data quality. All data were interpreted using Opus 4.2. Background subtraction, baseline correction, and normalisation were performed on all spectra. For the baseline correction, a linear baseline was subtracted over the range 4000–700 cm^{-1}. Normalisation was performed on baseline-corrected spectra over the range 1250–850 cm^{-1} and 1800–700 cm^{-1} for standards and bacterial samples, respectively. No further smoothing or manipulation was performed.

3. Results and discussion

3.1. Macroscale adsorption studies

3.1.1. Kinetics and reversibility

Cadmium kinetics experiments indicate that (1) adsorption equilibrium is rapid with full adsorption occurring in 45 min and (2) desorption is completely reversible reaching steady state in 30 min or less for all conditions investigated here (data not shown). These findings are in agreement with other studies of metal ion sorption onto bacterial surfaces (Fein et al., 1997; Fowle and Fein, 2000; Yee and Fein, 2001; Châtellier and Fortin, 2004; Borrok and Fein, 2005) and various algal biomass (Sheng et al., 2004). The fast rate of metal biosorption suggests that the sorption process is dependent solely on the electrostatic and chemical attraction between the metal and the functional groups present on the bacterial cell wall (Girault et al., 1998). The observed reversibility of adsorption justifies the use of equilibrium-based modeling approaches (Langmuir, 1997; Yee and Fein, 2001). Based on the results of these kinetic experiments, all subsequent batch adsorption experiments were conducted with an equilibration time of 2 h.

3.1.2. Cd adsorption onto Anoxybacillus flavithermus

The experimental data show that Cd adsorption increases with increasing pH, with negligible adsorption occurring below pH 4 (Fig. 1 displays data from a representative culture). This behaviour is attributed to the electrostatic attraction of Cd cations for anionic binding sites. Adsorption is enhanced at higher pH values due to increasing deprotonation of binding sites in or on the bacterial cell wall. Cadmium adsorption also increases with increasing bacterial concentration. This results from the increased total surface area of bacteria and effective increase in the total number of binding sites present in the suspension. Cadmium adsorption by *A. flavithermus* is similar to mesophilic bacteria; (Fein et al., 1997; Daughney and Fein, 1998; Daughney et al., 1998; Fowle and Fein, 1999; Daughney et al., 2001; Yee and Fein, 2003; Borrok et al., 2004a,b; Yee et al., 2004a,b; Borrok and Fein, 2005); the adsorption is strongly dependent on pH and controlled by the surface speciation of the bacterial cell wall.

We use FITMOD to develop SCMs to describe the experimental data. These SCMs include the deprotonation constants and site densities for the cell wall surface functional groups that were determined from acid-base titrations (Burnett et al., 2006), inferred to be carboxyl, phosphoryl, and amino structures (Table 1). For the purpose of this communication, the term 'one-site model' is used to describe SCMs in which the sorbate is assumed to interact with only one type of surface functional group, whereas in 'two-site models' the sorbate can interact with two different types of surface sites. A 'two-reaction model' is defined as an SCM in which the sorbate interacts with the cell surface via two different reaction mechanisms. These mechanisms may involve either one or two sites.

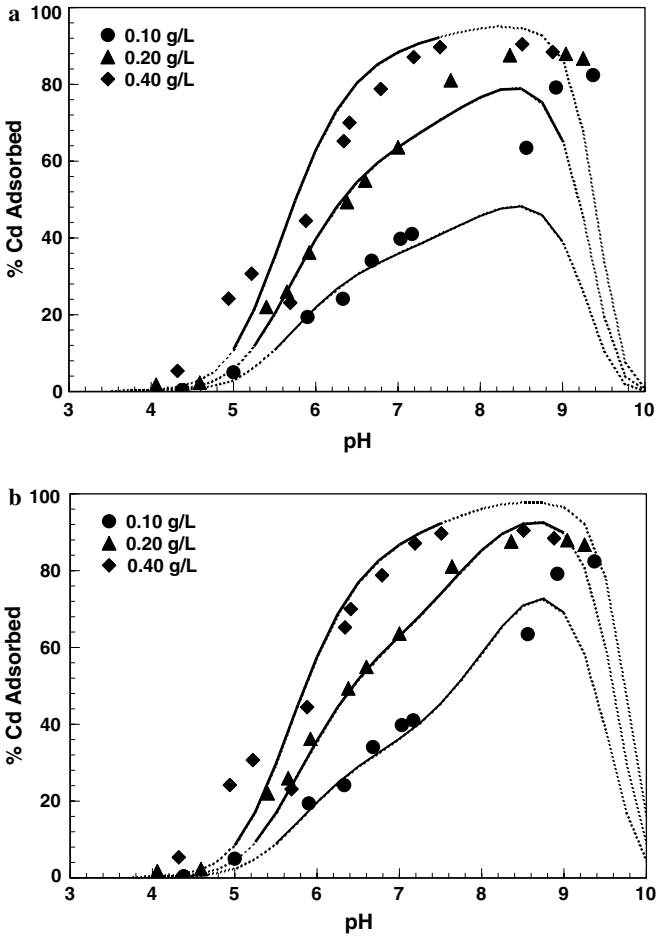

Fig. 1. A representative graph from a single culture of bacteria (trial 4, Table 2) with biomass concentration varied by dilution with the electrolyte. Biomass concentrations are quoted in dry gram per litre. Solid line represents model fit to the experimental data. Note that models are based on data with 10–90% adsorption and pH $\leqslant$ 9. Dashed line represents model prediction for conditions outside this range. (a) SCM includes only the unhydrolysed metal reacting with deprotonated carboxyl surface sites (Eq. 6). (b) SCM includes both the unhydrolysed metal and the first hydrolysis product of the metal reacting with deprotonated carboxyl surface sites (Eqs. 6 and 7).

Hence, an SCM that allows the formation of Cd–carboxyl ($RCOOCd^{+}$) and CdOH–carboxyl ($RCOOCdOH^{0}$) complexes would be termed a ''one-site two-reaction model''. For all SCMs, all Cd–bacteria surface complexes are assumed to have a 1:1 stoichiometry.

An SCM that considers only the adsorption of unhydrolysed Cd^{2+} onto deprotonated carboxyl sites (one-site one reaction model) provide an adequate fit to the experimental data when the Cd concentration is 5 mg L^{-1} and the bacterial concentration is above $\sim$0.25 dry g L^{-1} (Table 2). However, these one-site one reaction SCMs cannot sufficiently explain the observed adsorption behaviour exhibited in experiments conducted at lower bacteria-to-Cd ratios (5 mg L^{-1} Cd and bacterial concentrations below 0.2 dry g L^{-1}) (Fig. 1a). Similar findings have been reported by Fein et al. (1997), Daughney and Fein (1998), Daughney et al. (1998), Daughney

et al. (2001), and Ngwenya et al. (2003). Invoking a second reaction involving either adsorption of Cd^{2+} to deprotonated phosphoryl sites or the first hydrolysis product ($CdOH^{+}$) to deprotonated carboxyl or phosphoryl groups provides an excellent and significantly improved fit to all of the experimental data collected in this investigation (Table 2). In most instances, each of the three two-reaction SCMs proposed fit the adsorption data equally well and account for the enhanced adsorption effects in the upper pH region (Fig. 1b).

We then modeled all the data simultaneously with the aim of developing a single set of SCM parameters to describe all of the experimental data. The best-fitting SCM invoked the following two reactions:

Table 2
Adsorption of 5 mg L^{-1} Cd by *A. flavithermus* as modeled by FITMOD

Trial[a]	n[b]	g/L[c]	Metal Complexes	Log K_1[d]	Log K_2[e]	$V(Y)$[f]
1	28	1.09–0.25	$RCOOCd^{+}$	2.40	—	19.8
			RPO_4Cd^{+}	4.48	—	32.1
			$RCOOCd^{+}$, RPO_4Cd^{+}	No convergence[g]		
			$RCOOCd^{+}$, RCOOCdOH	No convergence[g]		
			$RCOOCd^{+}$, RPO_4CdOH	No convergence[g]		
2	19	0.62–0.15	$RCOOCd^{+}$	2.37	—	11.7
			RPO_4Cd^{+}	4.27	—	10.4
			$RCOOCd^{+}$, RPO_4Cd^{+}	2.16	3.47	7.46
			$RCOOCd^{+}$, RCOOCdOH	2.28	5.68	7.42
			$RCOOCd^{+}$, RPO_4CdOH	2.25	7.26	7.57
3	19	0.44–0.11	$RCOOCd^{+}$	2.26	—	3.57
			RPO_4Cd^{+}	4.07	—	4.97
			$RCOOCd^{+}$, RPO_4Cd^{+}	2.15	3.07	3.42
			$RCOOCd^{+}$, RCOOCdOH	2.16	5.93	3.38
			$RCOOCd^{+}$, RPO_4CdOH	2.18	7.31	3.14
4	25	0.40–0.10	$RCOOCd^{+}$	2.67	—	13.2
			RPO_4Cd^{+}	4.50	—	16.2
			$RCOOCd^{+}$, RPO_4Cd^{+}	2.50	3.42	10.5
			$RCOOCd^{+}$, RCOOCdOH	2.53	5.67	6.63
			$RCOOCd^{+}$, RPO_4CdOH	2.54	6.69	7.17
5	19	0.29–0.07	$RCOOCd^{+}$	2.37	—	2.56
			RPO_4Cd^{+}	4.22	—	7.48
			$RCOOCd^{+}$, RPO_4Cd^{+}	2.28	2.57	3.04
			$RCOOCd^{+}$, RCOOCdOH	2.28	5.35	3.07
			$RCOOCd^{+}$, RPO_4CdOH	2.32	5.68	2.74
6	11	0.20	$RCOOCd^{+}$	2.74	—	17.3
			RPO_4Cd^{+}	4.64	—	18.1
			$RCOOCd^{+}$, RPO_4Cd^{+}	2.62	3.44	17.5
			$RCOOCd^{+}$, RCOOCdOH	2.66	6.03	17.9
			$RCOOCd^{+}$, RPO_4CdOH	2.69	6.90	17.9
7	20	0.10	$RCOOCd^{+}$	2.64	—	19.7
			RPO_4Cd^{+}	3.79	—	23.0
			$RCOOCd^{+}$, RPO_4Cd^{+}	No convergence[g]		
			$RCOOCd^{+}$, RCOOCdOH	1.75	5.42	0.96
			$RCOOCd^{+}$, RPO_4CdOH	No convergence[g]		
ALL[h]	141	1.09–0.07	$RCOOCd^{+}$	2.46 ± 0.35	—	14.0
			RPO_4Cd^{+}	4.31 ± 0.56	—	18.7
			$RCOOCd^{+}$, RPO_4Cd^{+}	2.38 ± 0.39	2.93 ± 0.77	12.4
			$RCOOCd^{+}$, RCOOCdOH	2.38 ± 0.62	5.36 ± 0.50	10.2
			$RCOOCd^{+}$, RPO_4CdOH	2.39 ± 0.39	6.06 ± 1.33	10.3

[a] Single trial in which all Cd adsorption data are collected on bacterial cells from a single culture.
[b] Refers to the number of data points considered in construction of the SCM (only data between 10–90% adsorption and pH $\leqslant$ 9 were considered).
[c] Dry weight of bacteria per unit weight of electrolyte where parent suspension has been diluted to various concentrations covering the range noted. (Note that trials 6 and 7 were conducted at only one biomass concentration.)
[d] Log K value for cadmium adsorption forming the first type of surface complex included in the metal complex column, referenced to the condition of zero ionic strength and zero surface charge.
[e] Log K value for cadmium adsorption forming the second type of surface complex included in the metal complex column.
[f] Variance as calculated by FITMOD.
[g] Indicates severe misfit between the SCM and the experimental data.
[h] SCM parameters, with weighted 2σ errors, generated from modeling all data sets simultaneously.

$$R\text{–}COO^- + Cd^{2+} \Longleftrightarrow R\text{–}COOCd^+ \quad (6)$$

$$R\text{–}COO^- + CdOH^+ \Longleftrightarrow R\text{–}COOCdOH^0. \quad (7)$$

In no instance was a three-site or three-reaction SCM required to satisfactorily account for the observed adsorption (results not tabulated). This SCM yielded stability constants of 2.38 ± 0.62 and 5.36 ± 0.50 for the Cd–carboxyl and CdOH–carboxyl complexes, respectively. However, we stress that the other two-reaction SCMs fit most of the individual trials almost as well, and as such, identification of the second adsorption reaction mechanism (formation of a Cd–phosphoryl, CdOH–carboxyl, or CdOH–phosphoryl complex) is not possible based on the batch adsorption data alone. Hence, spectroscopic measurements are ultimately required to confirm the SCM reactions we have proposed (see below).

We graphically and statistically compared the SCM fit (above one-site two reaction SCM with overall variance of 10.2) to all of our experimental data using a bivariate scattergram (Fig. 2). Principal axes analyses were conducted using formulations described in Sokal and Rohlf (1995). The unbiased values for the slope (first eigenvalue of the variance–covariance matrix) and intercept of the principal axis of the relationship between the experimental data and the SCM predictions are 1.03 (0.99, 1.08) and −2.36 (−4.23, −0.56), respectively. (Values in the parentheses correspond to the 95% confidence intervals. The uncertainties in the slope and intercept were estimated using eigenvalues of the principal and secondary axes.) The degree of dissociation between the observed and predicted values was evaluated using the product-moment correlation coefficient (r) which was estimated at 0.96. The slope of this regression line is not significantly different from 1 and also overlaps (95% confidence interval) with its ideal value. Although the ideal value for the intercept (zero) lies outside the 95% confidence limits, the regression line is not significantly different from the $y = x$ line. Hence, based on principal axes analysis, the SCM is suitably accurate in view of our experimental uncertainties. Moreover, the SCM is able to match all of the experimental data to within approximately ±10%, covering a wide range of conditions from pH 3.6 to 9.0 and biomass concentration from 0.07 to 1.09 dry g L^{-1}.

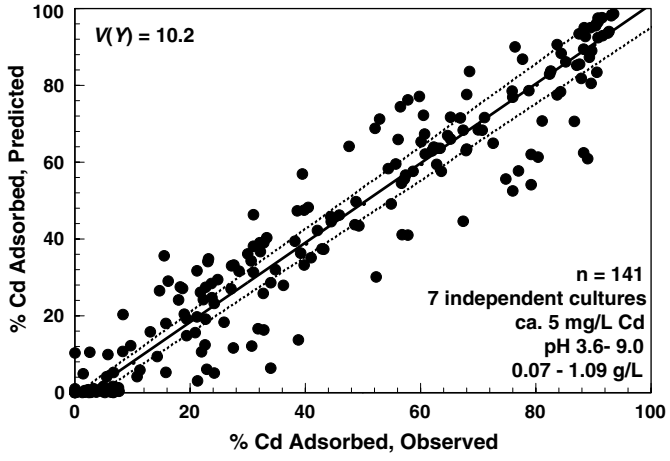

Fig. 2. Observed versus predicted extent of metal sorption, with predictions based on adsorption reactions given in Eqs. (6) and (7). $V(Y)$ is the variance between the SCM and the experimental data. Solid line is the linear regression line based on principal axes analysis and the dashed lines are the 95% confidence limits.

To examine whether the bacterial cells were affected by Cd, we measured DOC concentrations in filtrates after the bacterial suspensions were equilibrated for 2 h with Cd at various pHs (low, mid, and high) and ionic strengths (0.001, 0.01, and 0.1 M). Based on DOC analyses conducted on bacterial suspensions equilibrated at different pHs and ionic strengths during 2 h titrations (Burnett et al., 2006), the addition of 5 mg L^{-1} Cd had no significant effect on DOC concentrations after 2 h of equilibration, regardless of pH or ionic strength ($p > 0.05$). Confocal laser scanning microscopy examination indicates that most of the bacterial cells remain intact after equilibration with Cd. We assume that intact, non-viable cells will interact with ions identically to cells that are intact and viable, but metabolically inactive. Thus, we conclude that the presence of Cd does not affect the integrity of the cells of *A. flavithermus* under the conditions of our experiments.

3.2. XAS analyses

A small number of spectroscopic studies have been conducted to identify the functional groups on biological surfaces and those that are responsible for metal binding. Wei et al. (2004) found using ATR–FTIR that carboxylic, phosphate, and carbohydrate groups of both Gram-positive and Gram-negative bacteria were sensitive to changes in solution pH. Yee et al. (2004a,b) observed using synchrotron radiation FTIR that the cell surface functional groups on the cyanobacteria *Calothrix* are a combination of proteins, lipids, and carbohydrates. These authors also noted an increase in peak intensity at 1400 cm^{-1} over the pH range 3.2–6.5 during sequential titration of the cyanobacteria and concluded that these vibrational changes corresponded to the formation of deprotonated carboxyl sites. According to Kelly et al. (2001), uranyl binds to phosphoryl groups, whereas Cd binds to carboxyl functional groups on the surface of *Bacillus subtilis* at low pH. Uranyl has also been reported to interact with phosphoryl and carboxyl functional groups via inner-sphere complexation on the surface of *B. subtilis* (Kelly et al., 2002). Sarret et al. (1998) found via EXAFS that Zn binds predominantly to phosphoryl (95%) and minor carboxyl groups (5%) on *Penicillium chrysogenum*, but that Pb had a reversed affinity for the same surface. A study by Toner et al. (2005) also attributed Zn sorption by a bacterial biofilm to Zn–phosphoryl complexes, with a smaller contribution from carboxyl-type complexes. Independent investigations using X-ray Photoelectron Spectroscopy and FTIR revealed the chelating character of the ion coordination to carboxyl groups and confirmed that carboxyl, ether, hydroxyl, and amino

groups were responsible for the binding of Cd, Cu, Pb, Ni, and Zn by the marine algae *Padina sp.* and *Sargassum sp.* (Sheng et al., 2004). In summary, most previous investigations have concluded that carboxyl and phosphoryl sites play dominant roles in metal biosorption.

Both XANES and EXAFS data were collected of Cd adsorbed onto *A. flavithermus*. Spectra of Cd–perchlorate and Cd–acetate aqueous standards were also collected and will be used to explain the differences in XANES data that occur with complexation. The Cd–perchlorate standard was used as a proxy for free Cd^{2+} because Cd does not associate with ClO_4^- anions in solution. The amplitude reduction factor used throughout the fitting process was fixed at 0.96. Our XANES spectra of solution standards display a notable decrease of the white line intensity with increasing Cd–acetate complexation (Fig. 3a). A very subtle downshift in energy of all spectral features above the white line peak is also observed with increasing complexation. XANES of the Cd-biomass samples (Fig. 3b) are qualitatively similar to the near edge spectra of the Cd–acetate systems. As the pH of the biomass samples increase, there is also a reduction in the white line intensity, suggesting increasing complexation to "acetate-like" groups on the cell surface. As a result, the XANES suggests the participation of carboxyl functional groups in Cd binding by *A. flavithermus*. The EXAFS of the Cd–acetate systems agree with the XANES; pH increases are accompanied by a systematic reduction in the Cd–O peak height (Fig. 4a). Note that the Cd–C–C peak appears in the fully complexed Cd–acetate species due to multiple scattering arising from the linear configuration of the Cd and the two carbons in acetate. EXAFS of the Cd-biomass samples (Fig. 4b) also display a reduction in the Cd–O peak height (and increasing amplitudes of the second shell) with increasing pH. Fitting results of all samples (along with Cd surface loading) are summarised in Table 3. All Cd-biomass samples were successfully fitted with only the carboxyl ligand model. As such, the EXAFS not only corroborates the XANES, but more specifically, confirms the formation of the 1:1 Cd–carboxyl complex, the first reaction in our SCM for Cd adsorption by *A. flavithermus* (Eq. 6).

The increased Cd–O peak height in the EXAFS at low pH has been previously attributed to complexation with phosphoryl groups (Boyanov et al., 2003). However, it is possible that a small amount of free Cd^{2+} might affect the EXAFS spectrum of low pH (low sorption) samples. In our experiments, we utilised a lower concentration of Cd^{2+} specifically to avoid interferences from entrained aqueous Cd^{2+} and we did not observe any additional components at low pH. Thus, our results appear to differ from Boyanov et al. (2003), but we note that these authors used a different bacterial species and different bacteria-to-metal ratios, and as such, the binding chemistries observed would not necessarily be the same as for *A. flavithermus* under the conditions of the present investigation.

Based on the fitting of the EXAFS, the Cd complexation mechanisms between *A. flavithermus*, perchlorate, and acetate appear different (Fig. 5). Free Cd^{2+} exists in solution surrounded by six H_2O molecules with an average Cd–O bond distance of 2.27 Å. However, when Cd complexation to acetate ions is favourable, a stable bidentate mononuclear inner-sphere Cd–acetate complex (1:2) forms. This complex has average Cd–O, Cd–C, and Cd–C–C interactions of 2.28, 2.70, and 4.23 Å, respectively. From our studies, Cd

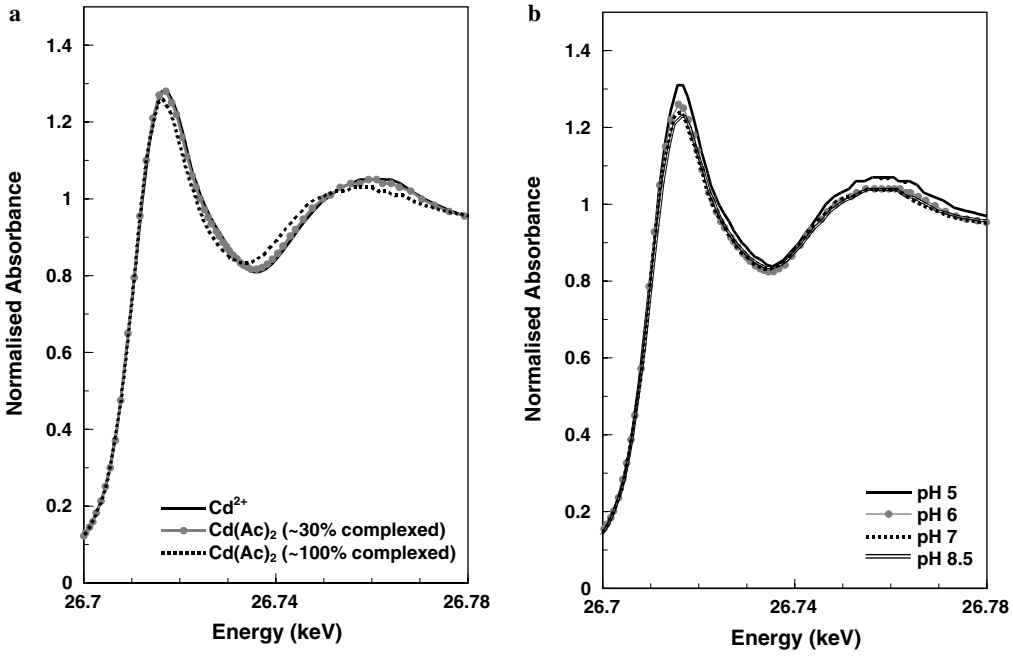

Fig. 3. Near edge spectra at the Cd K-edge. (a) Cd–perchlorate and Cd–acetate solutions. (b) Cd–*A. flavithermus* pastes at different pH values. Bacterial suspensions (~0.64 dry g L^{-1}) were exposed to ca. 5 mg L^{-1} Cd. The white line refers to the first most intense peak at the adsorption edge (~26.718 keV).

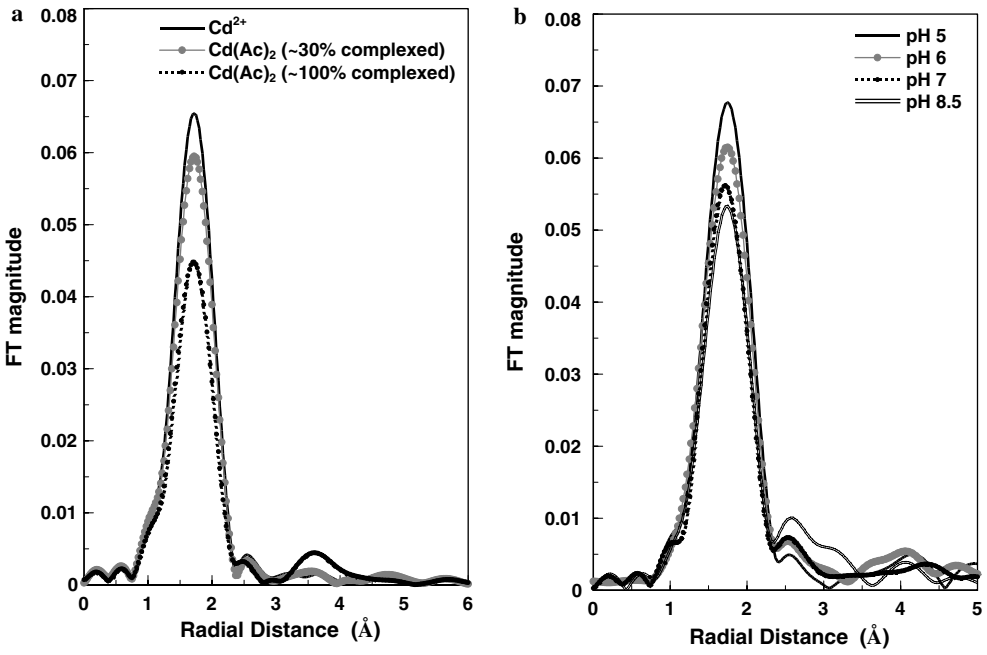

Fig. 4. Cd K-edge EXAFS RSFs. (a) Cd–perchlorate and Cd–acetate solutions. (b) Cd–*A. flavithermus* pastes at different pH values. Bacterial suspensions (~0.64 dry g L^{-1}) were exposed to ca. 5 mg L^{-1} Cd. For clarity only every second data point is plotted.

Table 3
Cd K-edge EXAFS curve-fitting results (with 2σ errors) for solution standards and biomass samples

Sample	Percent Cd sorbed[a]	Shell	*N*	*R*[b]	σ^{2}[c]	ΔE_0[d]
$Cd(ClO_4)_2$	—	Cd–O	6.6 ± 0.2	2.27 ± 0.00	7.9 ± 0.6	2.9 ± 0.2
$Cd(CH_3COO)_2$[e]	—	Cd–O	6.8 ± 0.7	2.28 ± 0.00	10.9 ± 1.4	7.1 ± 0.5
		Cd–C	1.3 ± 0.0	2.70 ± 0.02	7.2 ± 2.6	7.1 ± 0.5
		Cd–C–C	2.6 ± 0.5	4.23 ± 0.01	1.5 ± 0.0[f]	7.1 ± 0.5
pH 5[g]	36 (2.7)	Cd–O	6.8 ± 0.7	2.30 ± 0.01	5.9 ± 1.5	8.2 ± 1.1
		Cd–C	0.5 ± 1.7	3.19 ± 0.10	1.5 ± 8.5[f]	8.2 ± 1.1
pH 6[g]	71 (5.3)	Cd–O	6.4 ± 0.9	2.30 ± 0.01	6.3 ± 2.2	7.8 ± 1.5
		Cd–C	1.4 ± 0.2	3.19 ± 0.06	1.5 ± 0.0[f]	7.8 ± 1.5
pH 7[g]	91 (6.7)	Cd–O	6.5 ± 1.4	2.28 ± 0.02	7.7 ± 2.7	6.6 ± 2.9
		Cd–C	1.7 ± 0.5	3.22 ± 0.06	1.5 ± 2.9[f]	6.6 ± 2.9
pH 8.5[g]	93 (7.0)	Cd–O	6.2 ± 1.9	2.29 ± 0.02	8.0 ± 4.0	8.7 ± 3.1
		Cd–C	2.5 ± 1.2	3.20 ± 0.01	1.5 ± 0.0[f]	8.7 ± 3.1

[a] Percent Cd adsorbed onto biomass samples. Values in parentheses refer to the surface loading in $\times 10^{-3}$ mg Cd sorbed per Kg *A. flavithermus*.
[b] Radial distance in angstroms, Å.
[c] Disorder quoted in $\times 10^{-3}$ $Å^2$.
[d] Energy shift quoted in eV.
[e] Refers to cadmium acetate solution (pH 7.3) in which the cadmium is fully complexed.
[f] σ^2 factor constrained between 0.0015 and 0.01 $Å^2$.
[g] Biomass samples that had been exposed to 5 mg L^{-1} Cd.

interacts with carboxyl groups on the microbial surface by forming a monodentate mononuclear inner-sphere complex in which only one of the waters of hydration is lost. Across the pH range 5–8.5, the Cd–O and Cd–C bond distances vary slightly between 2.28–2.30 Å and 3.19–3.22 Å, respectively. These minimal shifts in bond distances suggest that the complexation mechanism in our experiments is unchanged over the pH range investigated and can be described adequately by carboxyl binding.

As previously discussed, the type and number of adsorption reactions occurring are dependent on bacteria-to-metal ratios at which experiments are performed, where high biomass samples need only invoke one adsorption mechanism, namely complexation of unhydrolysed Cd to carboxyl sites. As such, bacteria-to-metal ratios control the number of surface complexes that can be detected by spectroscopy. In our investigation, only one reaction mechanism is observed by XAS even at higher pH values, which is entirely consistent with the SCM. The samples used in the XAS experiments had a high bacteria-to-Cd ratio (~0.64 dry g L^{-1} exposed to 5 mg L^{-1} Cd), and thus, the SCM predicts only one adsorption mechanism (i.e.,

formation of the $RCOOCd^{+}$ complex). The spectroscopic data are consistent with the SCM, in that both indicate that Cd is complexed only by carboxyl sites under these experimental conditions. We emphasize that our results are not necessarily in conflict with previous studies that claim detection of more than one metal–bacteria surface complex by XAS (e.g., Sarret et al., 1998; Kelly et al., 2002; Boyanov et al., 2003; Toner et al., 2005). The Cd–carboxyl complex is the only one that can be verified under the conditions of our XAS experiments, but not necessarily the only complex that can possibly form under other experimental conditions.

3.3. FTIR analyses

Due to difficulty encountered in preparing samples for XAS that would allow detection of Cd–phosphoryl complexes (if any), a different approach was taken to elucidate the nature of surface complexes formed at lower bacteria-to-Cd ratios. Having already verified by XAS that Cd–carboxyl complexation occurs, we utilized FTIR to investigate the possibility of Cd–phosphoryl complexation as the second adsorption mechanism. FTIR analyses were conducted on a variety of phosphoryl compounds and directly on *A. flavithermus* in order to ascertain whether or not Cd–phosphoryl complexes form, and infer their possible importance in Cd biosorption.

The infrared spectra of aqueous PO_4^{3-}, HPO_4^{2-}, $H_2PO_4^{-}$, and H_3PO_4 are representative of the spectral changes that occur due to symmetry of a molecule (Fig. 6a). Recall that phosphoric acid has many deprotonation constants: pK_a of 2.1, 7.4, and 12.7 (Shriver and Atkins, 2003) and it is the protonation that significantly affects the molecular symmetry (Arai and Sparks, 2001). PO_4^{3-} belongs to the T_d point group and as such is expected to display a single strong v_3 stretching fundamental observed at 1004 cm^{-1}. Once PO_4^{3-} is protonated, the symmetry will be lowered. Systematic protonation to HPO_4^{2-} then $H_2PO_4^{-}$ results in C_{3v} and C_{2v} symmetry, respectively. The highest possible symmetry of the fully protonated H_3PO_4 is C_{3v}. Note that the lower the symmetry, the greater the band splitting of the infrared active bands. Vibrational frequencies and peak assignments are summarised in Table 4 and agree well with Persson et al. (1996) and Ross (1974).

The infrared spectrum of H_3PO_4 (50 mM) with Cd (1 M) at pH < 1 shows an intermediate behaviour between H_3PO_4 and $H_2PO_4^{-}$ (Fig. 6a). The C_{3v} peaks are characteristic of H_3PO_4 suggesting that the additional peaks probably arise from Cd complexing with phosphate. Smith and Martell (1976) recorded stability constants for the formation of $CdHPO_4$ (2.68) and CdH_2PO_4 (0.78) at 25 °C and an ionic strength of 3.0. Since the pH of the system was less than 1.0 in our experiments, the likely complex forming is

Table 4
The vibrational frequencies of phosphoryl standards

Sample	~pH	PO_4 symmetry	Frequency (vibrational mode)[a]
Inorganic P[b]			
50 mM H_3PO_4	<1.0	C_{3v}	1159 v (P=O); 1005 v_{as} (P–OH)
50 mM $H_2PO_4^{-}$	4.6	C_{2v}	1157 v_{as} (P–O); 1077 v_s(P–O); 940 v_{as} (P–OH); 882 v_s(P–OH);
50 mM HPO_4^{2-}	9.3	C_{3v}	1079 v_{as} (P–O); 990 v_s(P–O)
50 mM PO_4^{3-}	12.3	T_d	1004 v_{as} (P–O)
1 M Cd + 50 mM H_3PO_4	<1.0	C_{3v}, C_{2v}	1166 v (P=O)/v_{as} (P–O);1075 v_s (P–O); 1009 v_{as} (P–OH); 950 v_{as} (P–OH); 888 v_s(P–OH)
Organic P[c]			
50 mM $R_1R_2HPO_4$	2.6	C_s	1213 v (P=O); 1071 v (P–OH); 973; 925
50 mM $R_1R_2HPO_4$	3.8	C_s	1212 v (P=O); 1070 v (P–OH); 972; 928
50 mM $R_1R_2HPO_4$	6.6	C_s	1212 v (P=O); 1082 v (P–O); 1003; 972; 928
50 mM $R_1R_2HPO_4$	7.8	C_s	1213 v (P=O); 1082 v (P–O); 1003; 973; 927
50 mM $R_1R_2HPO_4$	10.5	C_s	1212 v (P=O); 1082 v(P–O); 1001; 973; 930
100 mM Cd + 50 mM $R_1R_2HPO_4$	7.5	C_s	1231 v(P–O); 1072 v(P–O); 999; 918
A. flavithemus[d]			
Bacterial pellet with and without exposure to 0.5 mM Cd	7.4	–	~1735 v(C=O) from lipids; ~1645 v(C=O) from Amide I; ~1546 δ (N–H) and v(C–N) from Amide II; ~1456 δ_{as} (CH_2) and δ_{as} (CH_3) from Amide III; ~1400 v_s(C–O) from carboxylic acids ~1240 v_{as}(P=O) from phosphodiesters and general phosphoryl groups ~1170 v(C–O) from polysaccharides ~1090 v_s(P–O) from phosphodiesters 1050–900 v(C–O) from polysaccharides

[a] Frequencies of vibrational bands in wavenumbers, cm^{-1}.
[b] Vibrational mode assignments taken from Persson et al. (1996) and Ross (1974).
[c] Only the two most intense peaks have been assigned (see text).
[d] Vibrational mode assignments taken from Kansiz et al. (1999), Giordano et al. (2001), Benning et al. (2004), and Yee et al. (2004a,b).

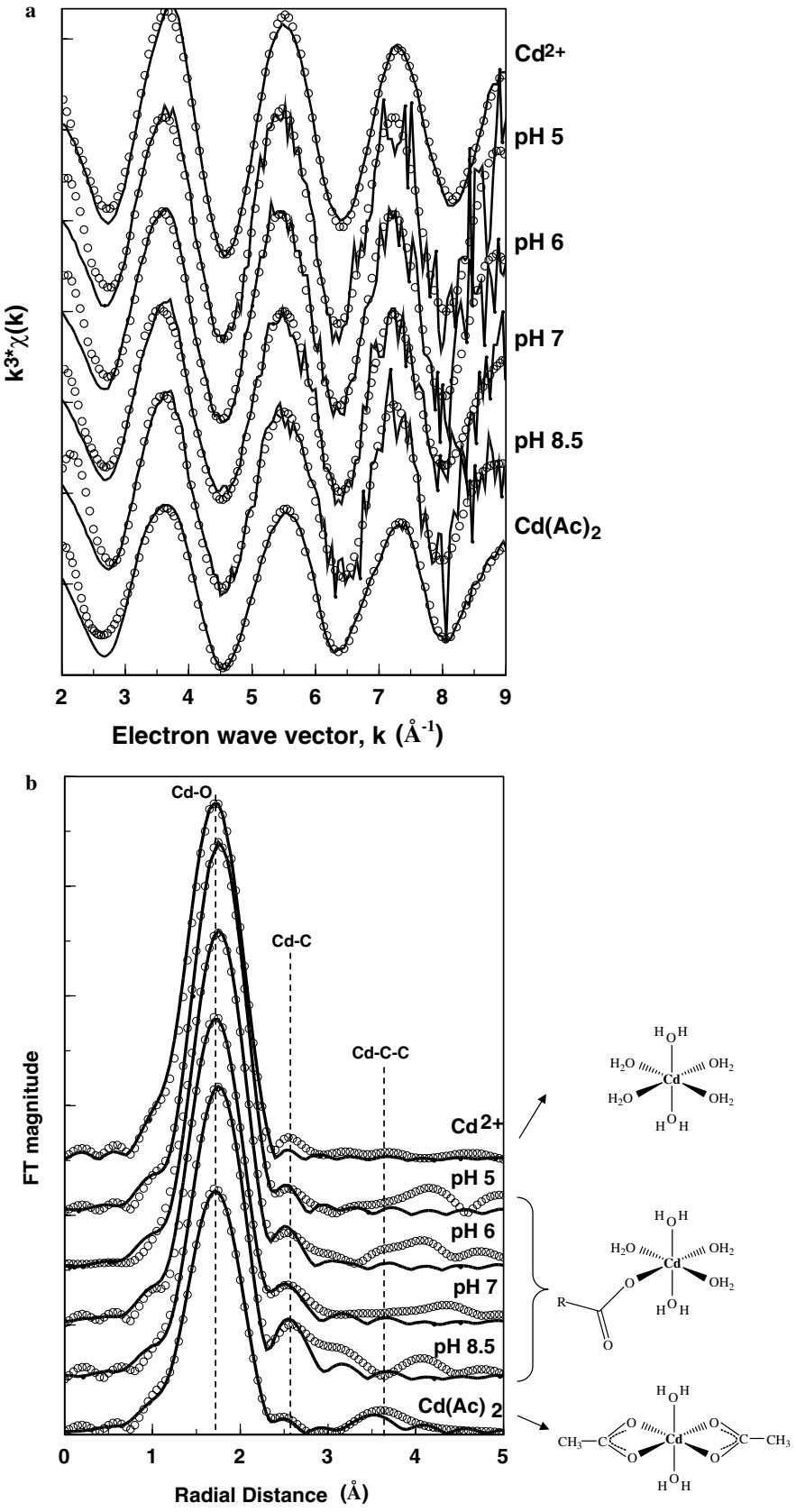

Fig. 5. Cd K-edge EXAFS for solution standards and all biomass samples. Note that the Cd–acetate species is fully complexed. (a) Data (lines) and fits (points) for $\chi(k)$ data. (b) Data (points) and fits (lines) for Fourier transform of $[k^3\chi(\mathrm{k})]$ data. For clarity only every second data point of the FT is plotted.

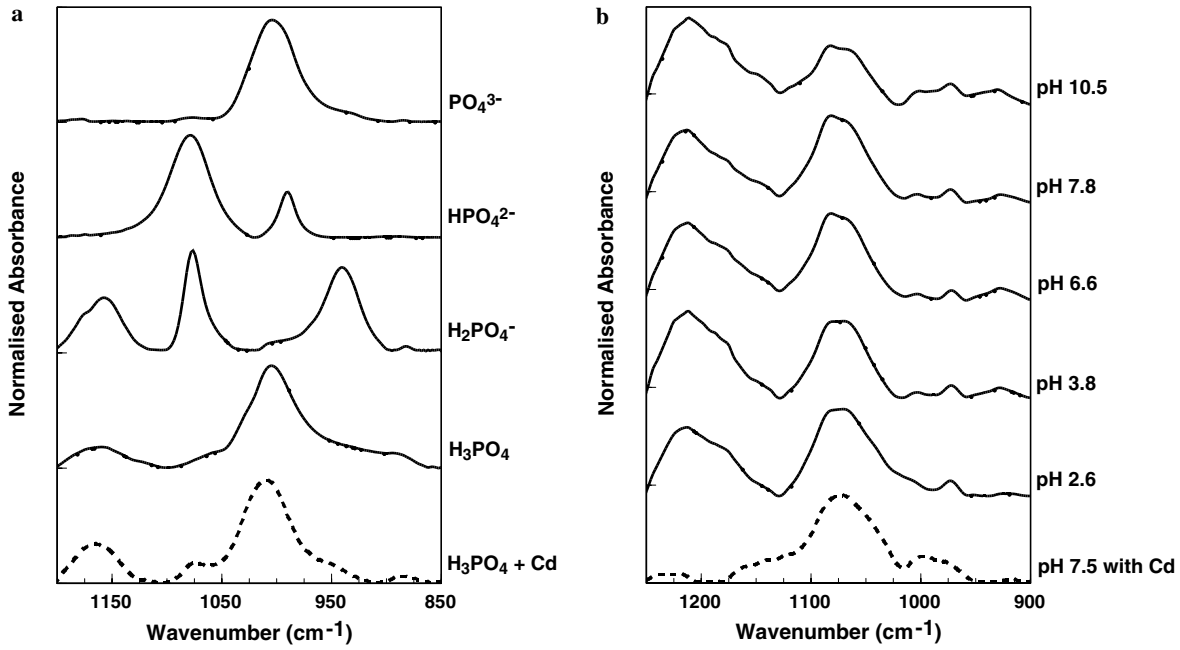

Fig. 6. Attenuated total reflectance FTIR spectra of phosphoryl standards. (a) Fifty millimolar solutions of PO_4^{3-}, HPO_4^{2}, $H_2PO_4^{-}$, H_3PO_4, and H_3PO_4 with 1 M Cd. (b) Fifty millimolar lecithin samples as a function of pH and a 50 mM lecithin sample with 100 mM Cd.

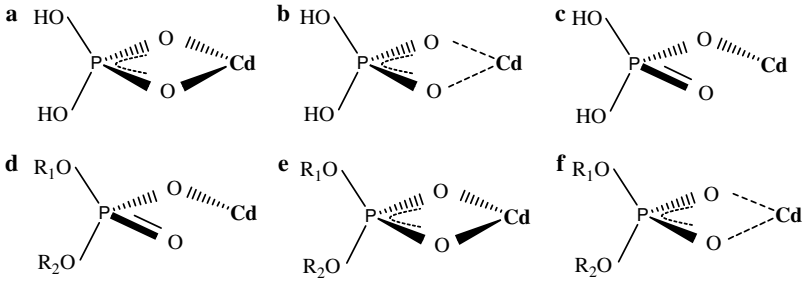

Fig. 7. Possible chemical structures for Cd–phosphoryl complexes. (a–c) Cd interactions with inorganic dihydrogen phosphate (bidentate inner-sphere, outer-sphere, and monodentate inner-sphere). (d–f) Cd interactions with lecithin (monodentate inner-sphere, bidentate inner-sphere, and outer-sphere).

CdH_2PO_4 from interaction of Cd with diprotic phosphate. The spectrum indicates that the complex has C_{2v} symmetry. However, we are unable to state conclusively whether the complex is inner-sphere (Fig. 7a) or outer-sphere (Fig. 7b). From Pearson's Hard Soft Acid Base (HSAB) classification, we would presume that Cd (a soft cation) forms outer-sphere complexes with oxygen donor ligands. This is supported by three-dimensional X-ray diffraction data which showed that Cd formed a 1:1 complex with the nucleotide guanosine 5′-phosphate via outer-sphere coordination (intramolecular H-bonds) with the phosphate group (Aoki, 1976). On the contrary, X-ray spectroscopic studies conducted by Boyanov et al. (2003) found that Cd formed an inner-sphere complex with phosphate when reacted in the Cd:PO_4 ratio of 1:5 (Fig. 7c). This proposed inner-sphere complex from Boyanov et al. (2003) does not possess C_{2v} symmetry and is therefore not consistent with peaks observed in our FTIR data.

The peak positions in the lecithin samples are shifted from inorganic phosphates because of the C_1 symmetry associated with organic phospholipids ($R_1R_2HPO_4$) (Fig. 6b). (Note that C_s symmetry could exist if the hydrocarbon chains possessed a mirror plane). The bands at $\sim$1212 cm^{-1} throughout all pure lecithin samples may correspond to the asymmetric P=O stretch (Table 4). For pH values less than 4, a peak at $\sim$1070 cm^{-1} is detected, whereas for pH values greater than 6.5, we observe a band at 1080 cm^{-1} (Fig. 6b). This difference at higher pH values could be a result of deprotonation of the phospholipid. Hence, we infer that the 1070 and 1080 cm^{-1} bands correspond to P–OH and P–O stretches, respectively. The infrared spectra changes only slightly with pH which is anticipated because the phospholipid maintains C_1 symmetry regardless of deprotonation. Assignments for the other bands tabulated in Table 4 have not been made because (1) the phospholipids have a complex structure, (2) inorganic

phosphate may not be a suitable model for comparison, and (3) these lower vibrational frequencies do not change with pH (or addition of Cd) and thus may not necessarily arise from phosphoryl vibrations. A more detailed analysis employing computational chemistry would be required in order to make further band inferences.

To determine if Cd interactions between inorganic phosphate and phospholipids are similar, we also collected spectra of lecithin samples (50 mM) containing Cd (100 mM). Significant differences in the intensities of the vibrational bands are observed (Fig. 6b) with the most obvious being the disappearance of the intense peak at $\sim$1213 cm^{-1}. A more subtle change is the position of the 1082 cm^{-1} peak shifting downwards by 10 cm^{-1} once Cd is introduced into the system. Assuming that the hydrocarbon side chains do not have a mirror plane, then a variety of possibilities exist for a Cd–phospholipid complex at pH 7.5 having C_1 symmetry (Figs. 7d–f). (Note that we are not excluding the formation of CdOH–phosphoryl complexes, though not illustrated.) If the band assignment of the asymmetric P=O stretch is correct, then the monodentate inner-sphere complex can be excluded (Fig. 7d). The formation of the outer-sphere complex (Fig. 7f) is the most likely candidate since Cd is a soft (polarisable) cation not predicted to form strong covalent bonds with oxygen ligands. This assignment is also in agreement with NMR studies on Cd interactions with phospholipids in model membranes (Girault et al., 1998). These authors found that Cd remained mostly uncomplexed in the bulk solution as free Cd^{2+} and that some Cd bound to anionic phospholipids forming 1:1 and 1:2 Cd–phospholipid complexes. They attributed the interactions as predominantly electrostatic (outer-sphere) because the binding could easily be reversed in high salinity or low pH conditions.

FTIR investigations suggest that the reaction mechanism of Cd with phosphoryl groups is similar between inorganic and organic phosphoryl ligands. However, neither inorganic phosphate nor organic phospholipids may be representative of phosphoryl functional groups on a cell surface. FTIR spectra were collected directly on *A. flavithermus* near neutral pH with and without 0.5 mM Cd (Fig. 8). A variety of functional groups were inferred (e.g., lipids, proteins, polysaccharides, and nucleic acids) in which the phosphoryl groups were relatively consistent with the wavenumbers from the phospholipids standard (Table 4). There were no obvious differences between the spectra, although peak intensities were greater for the sample not exposed to Cd. Dampening effects in the spectrum of the bacteria exposed to Cd may have resulted from spectral subtraction of the background solution. Additionally, there were slight shifts in wavenumbers of the phosphoryl bands ($\sim$1240 and $\sim$1090 cm^{-1}). However, these spectral regions overlap with NO_3^- vibrations from our background electrolyte, and conclusive information cannot be obtained regarding Cd complexation to phosphoryl sites on the cell wall. These results do not indicate that Cd–phosphoryl coordination does not occur on our microorganism, but rather that we were unable to conclusively observe this type of binding mechanism using FTIR.

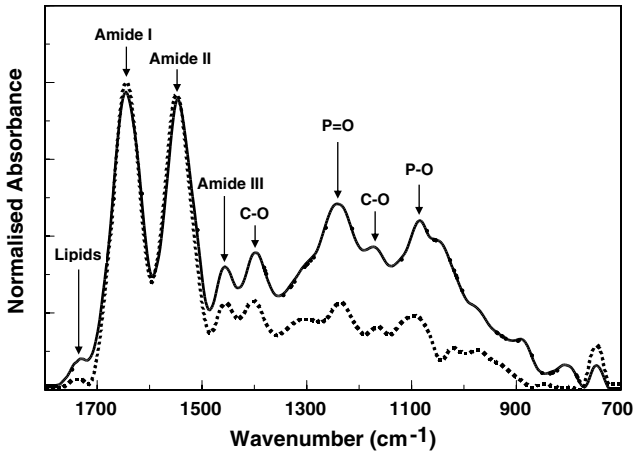

Fig. 8. Attenuated total reflectance FTIR spectra of *A. flavithermus* pastes. Bacterial suspensions ($\sim$0.2 dry g L^{-1}) equilibrated at pH 7.4 with (dotted line) and without (solid line) 0.5 mM Cd.

3.4. Comparisons to other bacteria

The SCM parameters compiled in Table 5 were used as a basis for comparison of Cd adsorption by various biological surfaces. The SCM curve describing Cd adsorption by *A. flavithermus* (based on Eqs. (6) and (7) and stability constants compiled in Table 2) was compared to Cd adsorption SCM curves for (1) the Gram-positive mesophile *B. subtilis* (Daughney et al., 2001), (2) the Gram-negative mesophile *Escherichia coli* (Yee and Fein, 2001), (3) the Gram-negative mesophile *Pseudomonas mendocina* (Borrok and Fein, 2005), and (4) six natural consortia from Borrok et al. (2004a). Note that cells of *B. subtilis* and *E. coli* were exposed to acidic solutions prior to experimentation. Thus, comparisons should be made with caution because acid-washing has been shown to increase the concentration of effective functional group sites (Borrok et al., 2004b). Note also that the six natural bacterial consortia were unique, with each consortium being a mixture of three to six species (Borrok et al., 2004a). Bacterial cells in the natural consortia were cultured at room temperature, whereas *E. coli*, *P. mendocina*, and *B. subtilis* were cultured at 37 °C. To our knowledge, there are no previous published SCMs for Cd adsorption by a thermophilic bacterium available for comparison to the results presented in this communication.

In general, the Cd adsorption behaviour of *A. flavithermus* is similar in style to the mesophilic bacteria that have been studied to date. For a given biomass concentration and at pH < ca. 8.5, *A. flavithermus* adsorbs less Cd than the pure cultures of mesophiles *B. subtilis*, *E. coli*, *P. mendocina* that have been maintained in the laboratory (Fig. 9). In contrast, *A. flavithermus* adsorbs more Cd than the

Table 5
The average characteristics of *A. flavithermus* and some other biological surfaces

Species	*A. flavithermus*	*B. subtilis*	*E. coli*	*P. mendocina*	Six natural consortia
Source	This paper	Daughney et al. (2001)	Yee and Fein (2001)	Borrok and Fein (2005)	Borrok et al. (2004a)
Model[a]	3 p*K*/Donnan	3 p*K*/Constant capacitance	1 p*K*/Constant capacitance	4 p*K*/Non-electrostatic	4 p*K*/Non-electrostatic
pK_1[b]	—	—	—	2.86 ± 0.38	3.12 ± 0.26
pK_2	4.94 ± 0.34	4.80 ± 0.10	4.87	4.66 ± 0.14	4.70 ± 0.22
pK_3	6.85 ± 0.57	6.49 ± 0.30	—	6.33 ± 0.14	6.57 ± 0.34
pK_4	7.85 ± 0.26	8.52 ± 0.60	—	9.04 ± 0.08	8.99 ± 0.42
C_1[c]	—	—	—	4.54 ± 1.47	3.33 ± 1.96
C_2	5.33 ± 0.87	6.92 ± 3.98	22.4	5.55 ± 0.24	3.39 ± 2.65
C_3	1.79 ± 0.84	4.44 ± 2.65	—	3.02 ± 0.18	1.84 ± 1.71
C_4	1.42 ± 0.29	6.29 ± 2.24	—	2.57 ± 0.12	2.24 ± 2.19
C_T[d]	8.54 ± 2.00	17.6 ± 8.9	22.4	15.7 ± 2.0	10.8 ± 8.5
$\log K_{Cd\text{-}1}$[e]	—	—	—	—	2.83 ± 0.60
$\log K_{Cd\text{-}2}$	2.38 ± 0.62	3.62 ± 0.50	3.870	4.01	2.70 ± 0.94
$\log K_{Cd\text{-}3}$	—	4.11	—	4.77	3.95 ± 0.44
$\log K_{Cd\text{-}4}$	—	—	—	—	5.22 ± 0.80
$\log K_{CdOH\text{-}1}$	5.36 ± 0.50	—	—	—	—

[a] SCMs consider one, three, or four distinct types of surface functional groups and are termed 1 p*K*, 3 p*K*, and 4 p*K*, respectively, surface electric field was accounted for using the Donnan or Constant capacitance model; Borrok et al. (2004a) and Borrok and Fein (2005) did not account for electrostatic effects.

[b] Negative logarithm of the stability constant describing deprotonation of the subscripted functional group, with 2σ errors, corresponding to the condition of zero ionic strength and zero surface charge; Yee and Fein (2001) did not report errors for all model variables.

[c] Absolute concentrations of the subscripted surface functional groups, with 2σ errors, in $\times 10^{-4}$ moles per gram of dry bacteria; Yee and Fein (2001) did not report all errors.

[d] Total site density, with 2σ errors, in $\times 10^{-4}$ moles per gram of dry bacteria.

[e] Log *K* value for cadmium adsorption, with 2σ errors, referenced to the condition of zero ionic strength and zero surface charge; The subscripted group refers to the sorbate (Cd vs. CdOH) and the site to which it is adsorbing (site 1 vs. site 2 vs. site 3 vs. site 4). Daughney et al. (2001), Yee and Fein (2001), and Borrok and Fein (2005) did not report all errors.

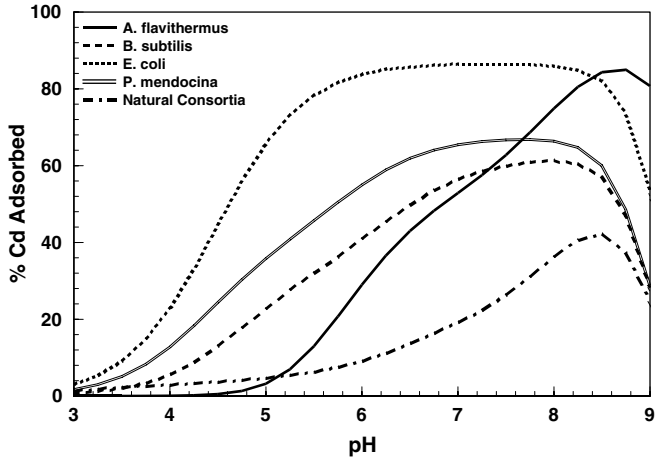

Fig. 9. FITMOD SCM output comparing the Cd adsorption behaviour of *A. flavithermus* to the mesophiles *B. subtilis* (Daughney et al., 2001), *E. coli* (Yee and Fein, 2001), *P. mendocina* (Borrok and Fein, 2005), and the average behaviour of six natural mesophilic bacterial consortia (Borrok et al., 2004a). The curves are calculated using the stability constants and surface site concentrations summarized in Table 5, assuming 0.2 dry gram of biomass per litre of solution and 5×10^{-5} M total Cd.

natural consortia of mesophilic bacteria (Borrok et al., 2004a), despite *A. flavithermus* possessing a lower total concentration of proton-active functional groups per unit weight of biomass.

Temperature may be responsible for the observed differences in metal adsorption between our thermophile and previously studied mesophiles. Temperature might influence metal adsorption in more than one way: (1) the effect of growth temperature on adsorption and (2) the effect of adsorption (reaction) temperature. Growth temperature is known to influence cell wall configuration (Denich et al., 2003; Sundaram, 1986), and we anticipate that these differences will result in different metabolic behaviours and subsequently different stability constants and site concentrations. Reaction temperature effects have been observed in the biosorption of Zn and Pb onto *P. aeruginosa* and *Dunaliella tertiolecta* (Ledin, 2000). The data displayed increased metal adsorption with increasing adsorption temperature. However, experiments on *B. subtilis* at elevated temperatures suggest that reaction temperature has minimal effects on the acidity constants of the surface functional groups (Wightman et al., 2001). These experiments demonstrated that a single set of acidity constant values and the site abundances for a particular bacterial species can adequately account for protonation behaviour over the temperature range 30–75 °C. Although these authors did not investigate metal adsorption, shifts in proton adsorption are likely comparable to shifts in metal adsorption. Thus, there are discrepancies in the scientific literature of reaction temperature effects on metal adsorption. Overall, temperature effects might be significant, but are outside the scope of the current paper.

4. Conclusions

Geochemical modeling of macroscopic adsorption data yields stability constants of metal–bacteria complexes, but the actual adsorption mechanisms remain inferences. Our batch adsorption studies revealed that the Cd adsorption behaviour of *A. flavithermus* is analogous to that observed for previously studied mesophilic bacteria, despite the reconfiguration of thermophilic cell wall composition in response to growth temperature (e.g., Briandet et al., 1999; Mattarelli et al., 1999). Not only is Cd biosorption by *A. flavithermus* strongly dependent on pH and controlled by the surface speciation of the bacterial cell wall, but the nature of binding reactions is also affected by bacteria-to-Cd concentration ratios. Like us, Fein et al. (1997) and Daughney et al. (1998) observed that at high bacteria-to-metal ratios, SCMs that consider formation of only Cd–carboxyl complexes were adequate to describe the data. They inferred that deprotonated carboxyl groups acted as primary binding sites, but that under low bacteria concentrations, where those sites are already saturated with metal at low pH, then the metal will bind to secondary sites under higher pH conditions. They attributed the secondary sites to deprotonated phosphoryl groups and the second important reaction to formation of Cd–phosphoryl complexes. On the other hand, the interaction of the positively charged first metal hydrolysis product (MOH^+) with a deprotonated carboxyl site has been suggested as a third reaction mechanism for the adsorption of Cu and Pb onto *B. subtilis* (Fowle and Fein, 1999). We have developed three different types of two reaction SCMs (formation of a Cd–carboxyl complex with either a Cd–phosphoryl, CdOH–carboxyl, or CdOH–phosphoryl complex) which all fit the data equally well. Considering only batch adsorption data, it is impossible to determine which of these three two-reaction SCMs is most appropriate (i.e., most accurate and realistic) and we acknowledge that we are in fact unable to identify the "best-fitting" one.

We relied on XAS data to provide electronic and structural information on each Cd–bacteria complex formed. However, based on the biomass concentration used to prepare the XAS samples (and essentially the bacteria-to-Cd ratio), only the formation of the 1:1 Cd–carboxyl complex could be verified. Based on (1) our FTIR data of model phosphoryl compounds, (2) NMR studies conducted by Girault et al. (1998), and (3) X-ray diffraction data collected by Aoki (1976), the formation of outer-sphere Cd–phosphoryl complexes on bacterial surfaces appears plausible. However, FTIR data of *A. flavithermus* exposed to Cd did not provide direct evidence of this adsorption reaction mechanism.

Although XAS should be able to distinguish between different ligands bonding to metals in biomass, we have demonstrated that it is extremely important to perform experiments with an appropriate bacteria-to-metal ratio, because it determines the adsorption mechanism. To verify the nature of the second adsorption reaction proposed in our SCM, the best experimental conditions for XAS analyses would require significantly lower bacteria-to-Cd ratios than we have employed in this study. However, it is experimentally difficult to select a bacteria-to-metal ratio that results in sufficiently high metal surface loading, while simultaneously retaining a low metal concentration in the entrained solution to optimise spectroscopic resolution. Note that even if Cd–phosphoryl complexation is plausible under low bacteria-to-Cd ratios, it is not expected to be detectable with XAS if it proceeds via an outer-sphere mechanism. This is because the Cd–P interatomic distance would be too long to model. Future spectroscopic studies will be conducted at lower bacteria-to-Cd ratios as physiochemical conditions of the system are varied, and utilizing other metals and thermophilic bacteria both in single and multicomponent systems. These studies will also be directed at studying the effects of temperature (and metabolism) on metal adsorption.

Acknowledgments

We thank Barry Goetz, Kim Handley, Jennifer Fernet, John Lawrence, Bruce Mountain, Marshall Muller, Chris Searle, and Arlette Seib with assistance in analytical work. Additionally, we thank the PNC-CAT beamline scientists at the Advanced Photon Source, Illinois, for assistance with experimental setup. This manuscript was greatly improved by the critical reviews of the Associate Editor and three anonymous referees. This research was funded by the New Zealand Foundation for Research, Science and Technology (Contract C05X0303: Extremophilic Microorganisms for Metal Sequestration from Aqueous Solutions) and made possible by a Research Tools and Instrument grant from the Natural Sciences and Engineering Council of Canada (NSERC).

Associate editor: Liane G. Benning

References

Aoki, K., 1976. Crystallographic studies of interactions between nucleotides and metal-ions. II. Crystal and molecular-structure of 1:1 complex of cadmium(II) with guanosine 5'-phosphate. *Acta Crystallogr B* **32**, 1454–1459.

Arai, Y., Sparks, D.L., 2001. ATR–FTIR spectroscopic investigation on phosphate adsorption mechanisms at the ferrihydrite–water interface. *J. Colloid Interface Sci.* **241**, 317–326.

Benning, L.G., Phoenix, V.R., Yee, N., Tobin, M.J., 2004. Molecular characterization of cyanobacterial silicification using synchrotron infrared micro-spectroscopy. *Geochim. Cosmochim. Acta* **68**, 729–741.

Beveridge, T.J., Forsberg, C.W., Doyle, R.J., 1982. Major sites of metal binding in *Bacillus licheniformis* walls. *J. Bacteriol.* **150**, 1438–1448.

Borrok, D., Fein, J.B., Kulpa, C.F., 2004a. Proton and Cd adsorption onto natural bacteria consortia: testing universal adsorption behaviour. *Geochim. Cosmochim. Acta* **68**, 3231–3238.

Borrok, D., Fein, J.B., Tischler, M., O'Loughlin, E., Meyer, H., Liss, M., Kemner, K.M., 2004b. The effect of acidic solutions and growth conditions on the adsorptive properties of bacterial surfaces. *Chem. Geol.* **209**, 107–119.

Borrok, D.M., Fein, J.B., 2005. The impact of ionic strength on the adsorption of protons, Pb, Cd, and Sr onto the surfaces of Gram-negative bacteria: testing non-electrostatic, diffuse, and triple-layer models. *J. Colloid Interface Sci.* **286**, 110–126.

Boyanov, M.I., Kelly, S.D., Kemner, K.M., Bunker, B.A., Fein, J.B., Fowle, D.A., 2003. Adsorption of cadmium to *Bacillus subtilis* bacterial cell walls: a pH-dependent X-ray absorption fine structure spectroscopy study. *Geochim. Cosmochim. Acta* **67**, 3299–3311.

Briandet, R., Meylheuc, T., Maher, C., Bellon-Fontaine, M.N., 1999. Listeria monocytogenes Stott A: cell surface charge, hydrophobicity, and electron donor and acceptor characteristics under different environmental growth conditions. *Appl. Environ. Microbiol.* **65**, 5328–5333.

Brock, T.D., 1986. Introduction: an overview of the thermophiles. In: Brock, T.D. (Ed.), *Thermophiles: General, Molecular, and Applied Microbiology*. John Wiley and Sons Inc., pp. 1–16.

Burnett, P.-G., Heinrich, H., Peak, J.D., Bremer, P.J., McQuillan, A.J., Daughney, C.J., 2006. The effect of pH and ionic strength on proton adsorption by the thermophilic bacterium *Anoxybacillus flavithermus*. *Geochim. Cosmochim. Acta.* **70**, 1914–1927.

Chapelle, F.H., 2001. *Ground-Water Microbiology and Geochemistry*. John Wiley and Sons, Inc., New York.

Châtellier, X., Fortin, D., 2004. Adsorption of ferrous ions onto *Bacillus subtilis* cells. *Chem. Geol.* **212**, 209–228.

Daughney, C.J., Fein, J.B., 1998. The effect of ionic strength on the adsorption of H^+, Cd^{2+}, Pb^{2+}, and Cu^{2+} by *Bacillus subtilis* and *Bacillus licheniformis*: a surface complexation model. *J. Colloid Interface Sci.* **198**, 53–77.

Daughney, C.J., Fein, J.B., Yee, N., 1998. A comparison of the thermodynamics of metal adsorption onto two common bacteria. *Chem. Geol.* **114**, 161–176.

Daughney, C.J., Fowle, D.A., Fortin, D., 2001. The effect of growth phase on proton and metal adsorption by *Bacillus subtilis*. *Geochim. Cosmochim. Acta* **65**, 1025–1035.

Daughney, C.J., Châtellier, X., Chan, A., Kenward, P., Fortin, D., Suttle, C.A., Fowle, D.A., 2004. Adsorption and precipitation of iron from seawater on a marine bacteriophage (PWH3A-P1). *Mar. Chem.* **91**, 101–115.

Denich, T.J., Beaudette, L.A., Lee, H., Trevors, J.T., 2003. Effect of selected environmental and physico-chemical factors on bacterial cytoplasmic membranes. *J. Microbiol. Methods* **52**, 149–182.

Fein, J.B., Daughney, C.J., Yee, N., Davis, T.A., 1997. A chemical equilibrium model for metal adsorption onto bacterial surfaces. *Geochim. Cosmochim. Acta* **61**, 3319–3328.

Fein, J.B., Martin, A.M., Wightman, P.G., 2001. Metal adsorption onto bacterial surfaces: development of a predictive approach. *Geochim. Cosmochim. Acta* **65**, 4267–4273.

Fowle, D.A., Fein, J.B., 1999. Competitive adsorption of metal cations onto two Gram-positive bacteria: testing the chemical equilibrium model. *Geochim. Cosmochim. Acta* **63**, 3059–3067.

Fowle, D.A., Fein, J.B., 2000. Experimental measurements of the reversibility of metal–bacteria adsorption reactions. *Chem. Geol.* **168**, 27–36.

Fowle, D.A., Fein, J.B., Martin, A.M., 2000. Experimental study of uranyl adsorption by *Bacillus subtilis*. *Environ. Sci. Technol.* **34**, 3737–3741.

Giordano, M., Kansiz, M., Heraud, P., Beardall, J., Wood, B., McNaughton, D., 2001. Fourier transform infrared spectroscopy as a novel tool to investigate changes in intracellular macromolecular pools in the marine microalga Chaetoceros muellerii (Bacillariophyceae). *J. Phycol.* **37**, 271–279.

Girault, L., Boudou, A., Dufourc, E.J., 1998. ^{113}Cd-, ^{31}P-NMR and fluorescence polarization studies of cadmium(II) interactions with phospholipids in model membranes. *Biochim. Biophys. Acta (BBA)-Biomembranes* **1414**, 140–154.

Kansiz, M., Heraud, P., Wood, B., Burden, F., Beardall, J., McNaughton, D., 1999. Fourier transform infrared microspectroscopy and chemometrics as a tool for the discrimination of cyanobacterial strains. *Phytochemistry* **52**, 407–417.

Kelly, S.D., Boyanov, M.I., Bunker, B.A., Fein, J.B., Fowle, D.A., Yee, N., Kemner, K.M., 2001. XAFS determination of the bacterial cell wall functional groups responsible for complexation of Cd and U as a function of pH. *J. Synchrotron Radiat.* **8**, 946–948.

Kelly, S.D., Kemner, K.M., Fein, J.B., Fowle, D.A., Boyanov, M.I., Bunker, B.A., Yee, N., 2002. X-ray absorption fine structure determination of pH-dependent U-bacterial cell wall interactions. *Geochim. Cosmochim. Acta* **66**, 3855–3871.

Langmuir, D., 1997. *Aqueous Environmental Geochemistry*. Prentice Hall, Upper Saddle River, NJ.

Ledin, M., 2000. Accumulation of metals by microorganisms – processes and importance for soil systems. *Earth-Sci. Rev.* **51**, 1–31.

Madigan, M.T., 2000. Bacterial habitats in Extreme Environments. In: Seckbach, J. (Ed.), *Journey to Diverse Microbial Worlds*. Kluwer Academic Publishers, The Netherlands, pp. 63–74.

Martinez, R.E., Smith, D.S., Kulcycki, E., Ferris, F.G., 2002. Determination of intrinsic bacterial surface acidity constants using a Donnan shell model and a continuous pK_a distribution method. *J. Colloid Interface Sci.* **253**, 130–139.

Mattarelli, P., Biavati, B., Pesenti, M., Crociani, F., 1999. Effect of growth temperature on the biosynthesis of cell wall proteins from Bifidobacterium globosum. *Res. Microbiol.* **150**, 117–127.

Ngwenya, B.T., Sutherland, I.W., Kennedy, L., 2003. Comparison of the acid-base behaviour and metal adsorption characteristics of a Gram-negative bacterium with other strains. *Appl. Geochem.* **18**, 527–538.

Ohshima, H., Kondo, T., 1991. On the electrophoretic mobility of biological cells. *Biophys. Chem.* **39**, 191–198.

Ohshima, H., 1995. Electrophoretic mobility of soft particles. *Colloid Surf. A Physiochem. Eng. Asp.* **103**, 249–255.

Ohshima, H., 2002. Electrokinetic behaviour of particles: theory. In: Hubbard, A.T., Somasundran, P. (Eds.), *Encyclopedia of Surface and Colloid Science*. Marcel Dekker, New York, NY, pp. 1834–1852.

Persson, P., Nilsson, N., Sjoberg, S., 1996. Structure and bonding of orthophosphate ions at the iron oxide-aqueous interface. *J. Colloid Interface Sci.* **177**, 263–275.

Plette, A.C.C., van Riemsdijk, W.H., Benedetti, M.F., van der Wal, A., 1995. pH dependent charging behaviour of isolated cell walls of a Gram-positive soil bacterium. *J. Colloid Interface Sci.* **173**, 354–363.

Ross, S.D., 1974. Phosphates and other Oxy-anions of Group V. In: Farmer, V.C. (Ed.), *The Infrared Spectra of Minerals, Mineralogical Society*, London, pp. 383–422.

Sampson, M.I., Phillips, C.V., 2001. Influence of base metals on the oxidising ability of acidophilic bacteria during the oxidation of ferrous sulfate and mineral sulfide concentrates, using mesophiles and moderate thermophiles. *Miner. Eng.* **14**, 317–340.

Sarret, G., Manceau, A., Spadini, L., Roux, J.C., Hazemann, J.L., Soldo, Y., Eybert-Berard, L., Menthonnex, J.J., 1998. Structural determination of Zn and Pb binding sites in *Penicillium chrysogenum* cell walls by EXAFS spectroscopy. *Environ. Sci. Technol.* **32**, 1648–1655.

Sheng, P.X., Ting, Y.-P., Chen, J.P., Hong, L., 2004. Sorption of lead, copper, cadmium, zinc, and nickel by marine algal biomass: characterization of biosorptive capacity and investigation of mechanisms. *J. Colloid Interface Sci.* **275**, 131–141.

Shriver, D.F., Atkins, P.W., 2003. *Inorganic Chemistry*, third ed. W.H. Freeman and Company, New York.

Smith, R.M., Martell, A.E., 1976. *Critical Stability Constants. IV: Inorganic Complexes*. Plenum, New York, NY.

Sokal, R.R., Rohlf, F.J., 1995. *Biometry: The Principles and Practice of Statistics in Biological Research*, third ed. W.H. Freeman and Company, New York.

Stumm, W., Morgan, J.J., 1996. *Aquatic Chemistry: Chemical Equilibria and Rates on Natural Waters*. John Wiley & Sons Inc., New York.

Sundaram, T.K., 1986. Physiology and growth of thermophilic bacteria. In: Brock, T.D. (Ed.), *Thermophiles: General, Molecular, and Applied Microbiology*. John Wiley and Sons, Inc., New York, pp. 1–16.

Toner, B., Manceau, A., Marcus, M.A., Millet, D.B., Sposito, G., 2005. Zinc sorption by a bacterial biofilm. *Environ. Sci. Technol.* **39**, 8288–8294.

van der Wal, A., Norde, W., Zehnder, A.J.B., Lyklema, J., 1997. Determination of the total charge in cell walls of Gram-positive bacteria. *Colloid Surf. B Biointerfaces* **9**, 81–100.

Wasserman, E., Felmy, A.R., 1998. Computation of the electrical double layer properties of semipermeable membranes in multicomponent electrolytes. *Appl. Environ. Microbiol.* **64**, 2295–2300.

Wei, J., Saxena, A., Song, B., Ward, B.B., Beveridge, T.J., Myneni, S.C.B., 2004. Elucidation of functional groups on Gram-positive and Gram-negative bacterial surfaces using infrared spectroscopy. *Langmuir* **20**, 11433–11442.

Westall J.C., 1982. FITEQL: a computer program for the determination of chemical equilibrium constants from experimental data: Version 1.2, Report 82-01, Department of Chemistry, Oregon State University.

Wightman, P.G., Fein, J.B., Wesolowski, D.J., Phelps, T.J., Bénézeth, P., Palmer, D., 2001. Measurement of bacterial surface protonation constants for two species at elevated temperatures. *Geochim. Cosmochim. Acta* **65**, 3657–3669.

Wonders, H.A.M., van Leeuwen, H.P., Lyklema, J., 1997. Metal- and proton-binding properties of a core-shell latex: interpretation in terms of colloid surface models. *Colloids Surf. A Physiochem. Eng. Asp.* **120**, 221–233.

Yee, N., Fein, J.B., 2001. Cd adsorption onto bacterial surfaces: a universal adsorption edge? *Geochim. Cosmochim. Acta* **65**, 2037–2042.

Yee, N., Fein, J.B., 2003. Quantifying metal adsorption onto bacteria mixtures: a test and application of the surface complexation model. *Geomicrobiol. J.* **20**, 43–60.

Yee, N., Fowle, D.A., Ferris, F.G., 2004a. A donnan potential model for metal sorption onto *Bacillus subtilis*. *Geochim. Cosmochim. Acta* **68**, 3657–3664.

Yee, N., Benning, L.G., Phoenix, V.R., Ferris, F.G., 2004b. Characterization of metal-cyanobacteria sorption reactions: a combined macroscopic and infrared spectroscopic investigation. *Environ. Sci. Technol.* **38**, 775–782.